BSGF - Earth Sciences Bulletin 2024, 195, 12
© G. Baby *et al.*, Published by EDP Sciences 2024
https://doi.org/10.1051/bsgf/2024009

BSGF
Earth Sciences Bulletin
Available online at:
www.bsgf.fr

Open Access

The tectonostratigraphic latitudinal record of the eastern Red Sea margin

Guillaume Baby[1,*], Antoine Delaunay[1], Daniel Aslanian[2] and Abdulkader M. Afifi[1]

[1] Physical Science and Engineering Division, King Abdullah University of Science and Technology, Thuwal, Saudi Arabia
[2] Geo-Ocean, Ifremer, Université de Bretagne Occidentale, CNRS, 29280 Plouzané, France

Received: 6 November 2023 / Accepted: 12 April 2024 / Publishing online: 26 June 2024

Abstract – We characterize the eastern Red Sea necking crustal domain through its north-south structural and stratigraphic record. Along-strike margin segmentation occurred during rifting (~28-14 Ma), with tilted blocks filled by siliciclastic sediments structuring the northern poor-magmatic segment (28°N-21.5°N), while siliciclastic/volcanoclastic sediments and volcanic flows interpreted as SDRs characterize the southern magmatic segment (21.5°N−13°N). Tectonic and magmatic activity stopped in this crustal domain of the margin when a thick salt layer precipitated during the Middle Miocene (~14-13 Ma). The stratigraphy of the margin then became similar between the two segments suggesting comparable post-salt subsidence and common crustal characteristics throughout the Red Sea. By characterizing its tectonostratigraphic record on a regional scale, this study tests two end-member scenarios for the tectonic evolution of the Red Sea. It also provides new insights into the tectonostratigraphic record of a rift margin system by simultaneously comparing the evolution of a magma-rich and a magma-poor segment.

Keywords: Rifted margin / tectonostratigraphic record / magma-poor segment / magma-rich segment / Red Sea

Résumé – L'enregistrement tectonostratigraphique latitudinal de la marge orientale de la Mer Rouge. Nous caractérisons le domaine crustale d'étranglement de la marge orientale de la Mer Rouge par une analyse tectonostratigraphique de sa couverture sédimentaire. La marge est segmentée pendant la période de rift (~28-14 Ma) entre : (i) un segment nord (28°N-21,5°N) structuré par des blocs basculés vers le continent et remplis par des sédiments siliciclastiques ; (ii) un segment sud (21,5°N−13°N) associé à des prismes sédimentaires à vergences opposées de type SDRs, de composition sédimentaire mixte (siliciclastiques/volcanoclastiques) intercalée de coulées volcaniques. L'activité tectonique et magmatique de ce domaine crustal s'est arrêtée lors du dépôt d'une épaisse couche de sel massive au cours du Miocène moyen (~14-13 Ma). La stratigraphie de la marge est alors devenue homogène entre les deux segments, suggérant une subsidence post-dépôt du sel similaire et donc des caractéristiques crustales communes sur l'ensemble du domaine distal de la Mer Rouge. En caractérisant son enregistrement tectonostratigraphique à une échelle régionale, cette étude permet de tester deux scénarios opposés d'évolution tectonique de la Mer Rouge. Elle fournit également de nouvelles observations sur l'enregistrement tectonostratigraphique d'un système de marge de rift en comparant simultanément l'évolution d'un segment riche en magma et d'un segment pauvre en magma.

Mots clés : Marge de rift / enregistrement tectonostratigraphique / segment riche en magma / segment pauvre en magma / Mer Rouge

1 Introduction

The Gulf of Suez – Red Sea rifting initiated at ~30 Ma from the rotation of the Arabian Plate with respect to the Nubian Plate. A major shift in the pole of rotation occurred at ~14 Ma leading to the individualization of the Sinai Plate and the opening of the Red Sea *sensu stricto* (*e.g.*, Courtillot *et al.*, 1987; Le Pichon and Gaulier, 1988; Bosworth *et al.*, 2005). Three symmetric crustal domains emerge across the Red Sea from deep seismic data (wide-angle seismic profiles and teleseismic data) : a ~32-40 km thick proximal domain, a ~100 km wide necking domain, and a 4.5 km to 10 km thick distal domain, ranging in width from ~100 km to ~200 km

*Corresponding author: baby.guillaume@gmail.com

from north to south (Fig. 1A). Since the 1960s, two end-member tectonic models have been debated about the nature of the distal crustal domain. The "mainly rift" model (Fig. 1B) specifies that hyper-extended continental crust and exhumed continental mantle prevail throughout the Red Sea except for young oceanic crust (<5 Ma) restrained to the axial region in the south. In this scenario, the nature of the crust evolves gradually from north to south (*e.g.*, Bosworth *et al.*, 2005; Cochran, 2005; Stockli and Bosworth, 2019). The "mainly ocean" model (Fig. 1C) suggests that the Red Sea is floored from north to south by newly formed oceanic lithosphere since ~14-13 Ma (*e.g.*, McKenzie *et al.*, 1970; Izzeldin, 1987; Stern and Johnson, 2019; Augustin *et al.*, 2021; Delaunay *et al.*, 2023).

This ongoing debate on the nature of the distal crustal domain in the Red Sea is of significant scientific importance for a better understanding of rift-ocean transition processes. Beyond its scientific relevance, it also has important economic implications. A mainly continental distal crustal domain, as proposed by the "mainly rift" model, could potentially contain pre-rift sediments serving as source rocks for a petroleum system. This would significantly enhance the potential for hydrocarbon exploration of the northern Red Sea compared with the "mainly ocean" model, which assumes a neo-formed distal crustal domain. To date, investigations into the nature of this crustal domain have primarily relied on interpreting and modeling potential field data, leading to non-unique solutions (*e.g.*, Cochran, 2005; Augustin *et al.*, 2021; Le Magoarou *et al.*, 2021; Issachar *et al.*, 2023), and local studies based on the interpretation of deep seismic data (*e.g.*, Gaulier *et al.*, 1988; Egloff *et al.*, 1991; Ahmed *et al.*, 2013) and seismic reflection data with varying degrees of quality (*e.g.*, Izzeldin, 1987; Ali *et al.*, 2023a; Sang *et al.*, 2023; Delaunay *et al.*, 2023). No study has focused on the analysis of the sedimentary record of the Red Sea Basin on a regional scale that could bring new insights into the state of crustal thinning under the basin.

It is generally acknowledged that the tectonostratigraphic evolution of a rifted margin is separated into tectonic sequences with specific structural geometries and stratigraphic patterns (*e.g.*, Bally and Snelson, 1980; Aslanian *et al.*, 2009; Haupert *et al.*, 2016; Neuharth *et al.*, 2022). (I) The syn-rift sequence, related to crustal thinning, normal faulting, and growth strata during which two periods with specific accommodation rates are recognized (*e.g.*, Prosser, 1993; Gawthorpe and Leeder, 2000; Nutz *et al.*, 2022): (i) the rift initiation period, where the accommodation created by basement fault displacement is filled by sedimentation; and (ii) the rift climax, which corresponds to the period of maximum rate of displacement on a fault, where sedimentation is outpaced by the accommodation induced by the tectonic subsidence. (II) The transition sequence, marked by a progressive migration of the deformation towards the distal necking crustal domain. Post-tectonic geometries prevail in the proximal part of the necking domain while growth strata are deposited basinward (*e.g.*, Masini *et al.*, 2013; Pérez-Gussinyé *et al.*, 2020; Chenin *et al.*, 2022). (III) The post-rift sequence, where sedimentary accommodation is primarily driven by thermal subsidence of the oceanic lithosphere (*e.g.*, Steckler and Watts, 1978; Stein and Stein, 1992).

In theory, the characterization of these tectono stratigraphic sequences along the Red Sea margins could therefore provide

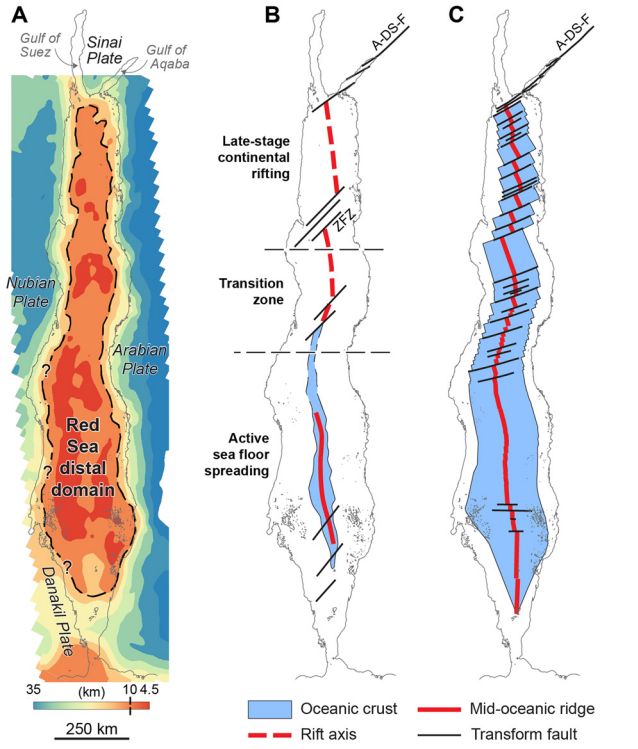

Fig. 1. (A) Crustal thickness map constructed by subtracting the basement from the moho depth maps (Supp. Data 1C and 1D). The hatched line is the 10 km iso-thickness marking the transition between the necking and the distal domains. (B) "Mainly rift" tectonic model redrawn from Bosworth (2015). (C) Mainly ocean tectonic model redrawn from Delaunay *et al.* (2023). A-DS-F: Aqaba-Dead-Sea Fault; ZFZ: Zabargad Fracture Zone. Projection system: Ain el Abd 1970, Aramco, Lambert 2. Rotation: −26.75°.

constraints on the state of crustal and lithospheric thinning beneath the Red Sea Basin over time and space, and highlight latitudinal variations as suggested by the "main rift" model. In practice, two challenges stand in the way. The first is the lithology of the basin, which includes an evaporite-rich interval with a thick layer of massive salt, deposited between ~16 and ~5 Ma (*e.g.*, Guennoc *et al.*, 1988; Beydoun, 1989; Mitchell *et al.*, 1992). By hampering geophysical signals, this evaporite unit will render difficult the interpretation of pre-salt and crustal geometries. The second is its territorial extension across five countries with overlapping economic interests, making it difficult to look at this system as a whole with a homogeneous dataset.

For the first time, we had access to a complete set of seismic reflection and well data in the Saudi waters, which penetrated the entire syn-rift pre-evaporites series. Combined with a review of the surface geology and previously published studies, these new data allow us to propose a comprehensive and coherent tectonostratigraphic evolution model at the regional scale for the entire eastern margin of the Red Sea. Although we are unable to conclude on the exact nature of the distal domain, we compare the evolution of the southern and northern Red Sea, providing new insights into the understanding of its geology and morphology.

2 Geological setting

2.1 Basement nature of the Red Sea

The uplifted Nubian-Arabian margins expose the Neoproterozoic continental basement made of amalgamated magmatic arcs overlain by sedimentary and volcanic basins, intruded by granitoids, and segmented by orthogonal to oblique shear zones and sutures (Fig. 2C) (*e.g.*, Stern and Johnson, 2019). These structures significantly affect the Red Sea rift geometry and are precursors to large-offset oceanic transform fault zones in the northern and middle Red Sea known respectively as the Zabargad and Jeddah fracture zones (Fig. 2B) (Molnar *et al.*, 2020 and references therein).

2.2 Geodynamic evolution of the Red Sea

The two main proposed drivers triggering Red Sea rifting are the slab-pull far-field extension of the subducting Arabian Plate below the Eurasian Plate (Bellahsen *et al.*, 2003) and the thermal weakening of the lithosphere due to the East-Africa hotspot track (Vicente de Gouveia *et al.*, 2018). Rifting started during the Oligocene and extended from the Gulf of Suez to the southern Red Sea (Bosworth *et al.*, 2005), contemporaneous with continental flood volcanism over a large part of north Ethiopia/Eritrea, northwest Yemen, and southwest Saudi Arabia (Bosworth and Stockli, 2016) at the triple junction between the Red Sea, the Gulf of Aden and the East-Ethiopian Rift (Fig. 2C). Backstripping methods applied to the Gulf of Suez show subsidence rates increase during the Early Miocene (~24-21 Ma) (*e.g.*, Moretti and Colletta, 1987) along with accelerated denudation along the Red Sea rift shoulders (*e.g.*, Bohannon *et al.*, 1989; Szymanski *et al.*, 2016), and intrusion of basaltic dikes and igneous complexes, and extrusion of several volcanic fields mainly along the eastern margin (*e.g.*, Sebai *et al.*, 1991; Korostelev *et al.*, 2015). Subsequently, during the Middle Miocene (~16-12 Ma), a plate reorganization resulted in the abandonment of the Gulf of Suez rift and motion transfer to the Aqaba-Dead Sea fault (*e.g.*, Courtillot *et al.*, 1987). This shift from normal to oblique extension coincides with the formation of the distal crustal domain of the Red Sea margins (Ali *et al.*, 2023a; Delaunay *et al.*, 2023). According to the two end-members scenarios about the nature of the crust in this domain, it would coincide with either the onset of seafloor spreading throughout the Red Sea ("mainly ocean" model – *e.g.*, Le Pichon and Gaulier, 1988; Delaunay *et al.*, 2023), or with the onset of hyperextension and eventually mantle exhumation ("mainly rift" model – *e.g.*, Ali *et al.*, 2023a). During the late Miocene (~13-8 Ma), the Danakil Block individualized from the Nubian Plate by a counter-clockwise rotation, partitioning the extension in the southern Red Sea (*e.g.*, McClusky *et al.*, 2010; Rime *et al.*, 2023). After ~12 Ma, and mostly during the Plio-Quaternary, the transitional-to-strongly-alkali volcanic fields (harrats) emplaced in a N-S trend over 1400 km in Saudi Arabia, Jordan, and Syria (*e.g.*, Camp and Roobol, 1992).

2.3 Tectonostratigraphic evolution of the Red Sea

The syn-rift and post-rift infill of the Red Sea is separated into three major sedimentary units that share similarities with the Gulf of Suez (*e.g.*, Montenat *et al.*, 1988; Purser and Hötzl, 1988; Beydoun, 1989; Mitchell *et al.*, 1992; Bosworth *et al.*, 2005).

2.3.1 Pre-evaporite Unit – Late Oligocene to Middle Miocene (~28-16 Ma)

This unit is associated with tilted blocks in the Gulf of Suez (Bosworth, 1995) locally imaged in the subsurface data from the Saudi margin of the northern Red Sea in: the Midyan Basin (Tubbs *et al.*, 2014), the Umluj Basin (Hughes and Johnson, 2005), and the offshore Azlam (Rowan, 2014) and Umluj (Mohriak, 2019) basins (Fig. 2A). In the southern Red Sea, Bohannon (1987) showed that the syn-rift sediments are concordant on the basement and tilted seaward. Seismic data available along the Tihama Plain confirms the absence of tilted blocks in this proximal domain of the margin (Doornenbal *et al.*, 1991; Davison *et al.*, 1994; Davison *et al.*, 1998). A recent study carried out at the southern end of the margin (Chauvet *et al.*, 2023) confirms that the syn-rift series were deposited as seaward-dipping reflector (SDR) volcanic wedges, commonly observed along passive volcanic margins.

Two syn-rift sequences locally separated by an Early Miocene-Middle Miocene unconformity are recognized in the Gulf of Suez and the Red Sea. The oldest is Late Oligocene to Early Miocene in age and is composed of alluvial "red beds", locally exposed in the coastal basins of the northern Red Sea. It is known as the Al Wajh Formation in Saudi Arabia (Hughes and Johnson, 2005), the Hamamit Formation in Sudan (Bunter and Abdel Magid, 1989), and the Abu Zemina Formation in Egypt (Bosworth, 1995). In the southern Red Sea, the early syn-rift sediments are exposed along the Ghawwas and Tihama coastal basins. They are composed of siliciclastic and volcanoclastic sediments (lacustrine deposits and pyroclastics) interbedded with lava flows, known as the Jizan Group in Saudi Arabia (Schmidt *et al.*, 1983) and as the Dogali Formation on the conjugate Eritrean margin (Sagri *et al.*, 1998). This early syn-rift period is interpreted as a "diffuse" deformation phase that resulted in a network of small grabens preserved on both sides of the northern Red Sea and Gulf of Suez (*e.g.*, Bosworth, 2015).

The second syn-rift sequence is Early to Middle Miocene and is marked by the installation of open marine environments in the Gulf of Suez together with an acceleration of the subsidence along the axis of the rift (*e.g.*, Moretti and Colletta, 1987; Evans, 1988; Rohais *et al.*, 2016). The first documented marine sediments in the eastern margin of the northern Red Sea include the Aquitanian carbonate platform of the Musayr Formation and the evaporites of the Yanbu Formation exposed in the inverted Midyan half-graben (Dullo *et al.*, 1983). These evaporites were dated by strontium isotopes in well samples from the Yanbu Basin at 23-21 Ma (Hughes and Johnson, 2005). Above, the Burqan Formation recorded marine clastic sedimentation (mainly turbidites and debris flows), exposed in the Midyan Basin and dated between biozones N5 and N8 (~22-16 Ma) (Hughes and Johnson, 2005). Similar marine series were drilled offshore in Egypt (Rudeis Formation) (*e.g.*, Bosworth *et al.*, 2005) and Sudan (Maghersum Group) (Bunter and Abdel Magid, 1989). Although poorly dated, potentially similar marine series were also drilled in Eritrea (Habab Formation) (Savoyat *et al.*, 1989).

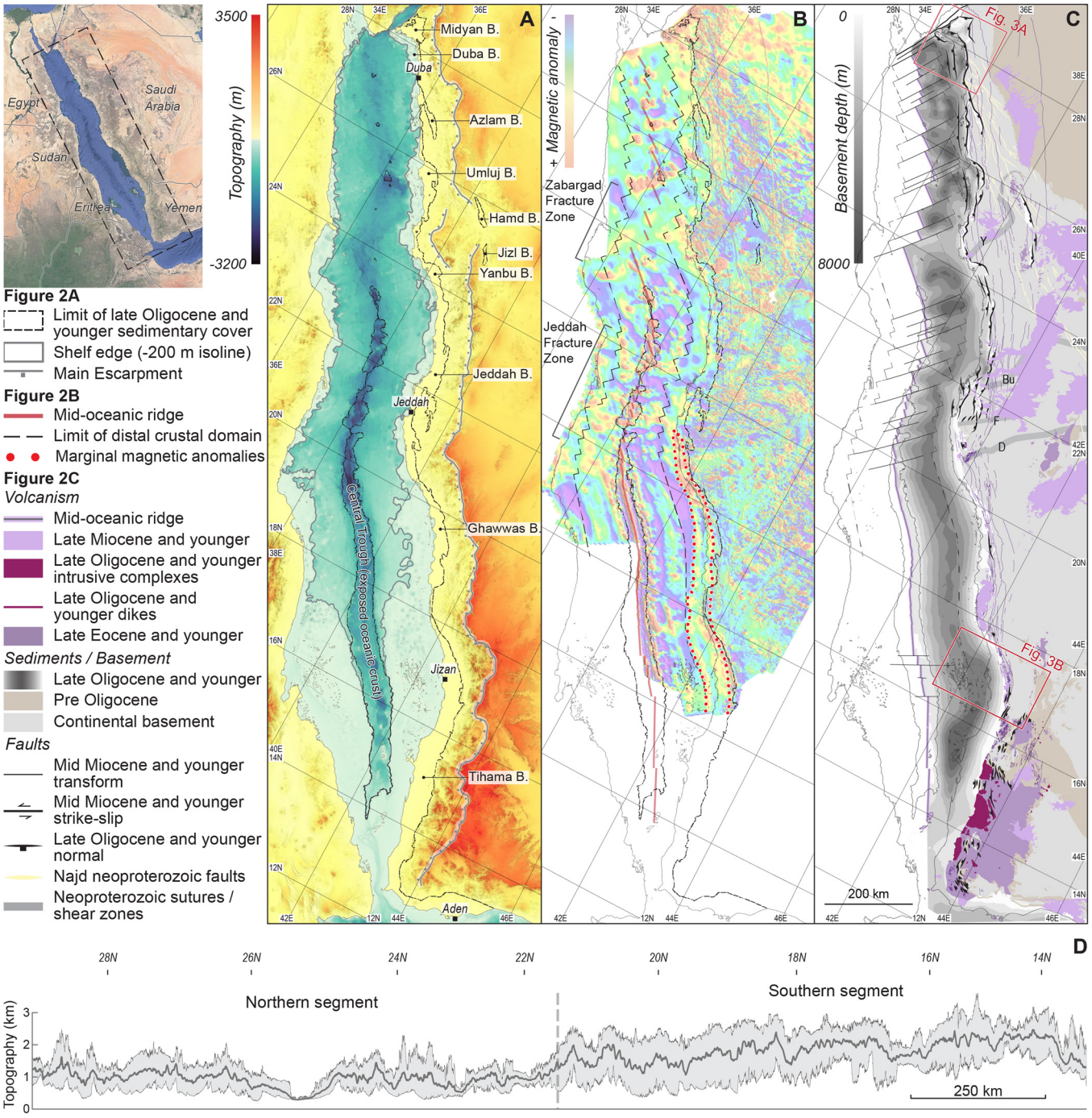

Fig. 2. (A) Morphologic elements and topography. The onshore basins of the eastern Red Sea rifted margin are named. (B) Offshore tectonic map (modified from Delaunay *et al.* (2023)) overlying magnetic survey. (C) Geological map and depth of the acoustic basement based on seismic reflection data. Shear zones and sutures from Stern and Johnson (2019). D: Ad Damm shear zone. F: Fatima shear zone. Bu: Bi'r Umq suture. Y: Yanbu suture. (D) Maximum, minimum, and mean elevation of the main escarpment over a 20 km swath profile. Digital elevation data from GEBCO (https://www.gebco.net/). Projection system: Ain el Abd 1970, Aramco, Lambert 2. Rotation: −26.75°.

However, no equivalence is known along the eastern margin of the southern Red Sea.

2.3.2 Evaporite Unit – Middle Miocene to Late Miocene (16-5 Ma)

Three successive evaporite-rich sub-units were deposited unconformably on the previous syn-rift sediments and the eroded basement. The first sub-unit is poorly defined in the Red Sea except in Saudi Arabia where it is known as the Maqna Group, well exposed in the Midyan Basin (Hughes and Johnson, 2005). It is composed of restricted marine deposits including clastics, carbonates, and evaporites (anhydrite). The proportion of evaporites increases through time indicating increasingly restricted marine environments. This unit is dated between N8 and N9b biozones (~16-14 Ma) (Hughes and Johnson, 2005). The equivalent formations from the Gulf of Suez are known as the Kareem and Belayim formations (*e.g.*, Evans, 1988).

The second unit is composed of massive halite only observed in subsurface data except locally with diapirs exposed along the Tihama Plain in the southern Red Sea (Davison *et al.*, 1996; Bosence *et al.*, 1998). It is known as the Mansiyah Formation in Saudi Arabia (Hughes and Johnson, 2005), South Garib Formation in Egypt (*e.g.*, Evans, 1988), Dungunab Formation in Sudan (Bunter and Abdel Magid, 1989), and Amber Formation in Eritrea (Savoyat *et al.*, 1989). This layer acts as a major detachment level that formed spectacular salt tectonics-related structures during the Late Miocene (*e.g.*, Heaton *et al.*, 1995; Rowan, 2014; Ali *et al.*, 2023b). It is little or not affected by basement faults and therefore interpreted respectively as a post-rift (Davison *et al.*, 1994) or a transition unit (Heaton *et al.*, 1995).

The third unit is composed of Middle to Late Miocene continental to transitional clastic sediments interbedded with evaporites (anhydrite) known as the Ghawwas Formation in Saudi Arabia (Hughes and Johnson, 2005), and Zeit Formation in Egypt (Evans, 1988). Its accommodation was highly controlled by salt tectonics. It is not affected by basement faults, except locally by strike-slip faults in the extension of the Gulf of Aqaba to the north of the Red Sea (*e.g.*, Stockli and Bosworth, 2019; Afifi *et al.*, 2023). This unit was dated between biozones N14 and N18 (Hughes and Johnson, 2005). Recent strontium isotope has suggested an older age for the onset of its deposition and constrained the Mansiyah massive salt layer between 14 Ma and 13.2 Ma (Pensa *et al.*, 2023).

2.3.3 Post-evaporite Unit – Pliocene to recent (5-0 Ma)

An uppermost Miocene (Messinian) regional erosional unconformity, previously defined throughout the Red Sea as the "S reflector" (Phillips and Ross, 1970), truncates the Evaporite Unit (*e.g.*, Mitchell *et al.*, 2021). Above, the Plio-Pleistocene sediments consist of open marine clastic sediments and aggrading carbonate platforms. They are defined as the Lisan Group in Saudi Arabia (Hughes and Johnson, 2005), the Post-Zeit Group in Egypt (*e.g.*, Evans, 1988), and the Abu Shagara Group in Sudan (Bunter and Abdel Magid, 1989). This post-rift unit is contemporaneous in age with the exposed oceanic crust along the axis of the southern Red Sea.

3 Data and method

New subsurface data coupled with geological mapping, previously published deep geophysical data, and magnetic data were used to study the eastern margin of the Red Sea and to unravel the architecture of its necking domain. Picking of regional seismic horizons and structural modeling were made with Move software. The various seismic surveys used in this study are located in Supp. Data 1.

3.1 Geological maps

The geological maps presented in this study (Figs. 2 and 3) are based on field observations, satellite images (Google Earth), and existing geological maps (Saudi National Geological Database (https://ngd.sgs.gov.sa/en) and the Geological Map of the Republic of Yemen (Kruck *et al.*, 1996)). The eastern Red Sea bounding faults were mapped using seismic reflection data. The dikes were mapped using aeromagnetic data from the Saudi Geological Survey (Zahran *et al.*, 2003). Neoproterozoic sutures/shear zones are from Stern and Johnson (2019).

3.2 Seismic reflection and well data

Four seismic reflection datasets were used to unravel the geometry of the margin (Supp. Data 1B). The first survey (proprietary, Saudi Arabia) was acquired with a set of 8 to 10 km-long streamers and processed through prestack depth migration. It has a spacing of ~30 to 50 km and extends from the coastal basins to the mid-oceanic ridge (total length ~11 000 km). The time depth conversion of this dataset was done using a multi-layered velocity model in order to illuminate subsalt targets. The second survey was acquired by CGG in 1976 and their interpretation was published by Izzeldin (1987). It consists of 16 cross-profiles, oriented N60 and spaced ~40 km apart, covering the central part of the Red Sea. The interpretation of these profiles was converted to depth by Mitchell *et al.* (2021) using a 3-layer velocity model. The third survey consists of interpolated depth-converted seismic data covering the northern half of the Yemeni part of the margin (Davison *et al.*, 1998). The fourth survey consists of 11 regional depth-converted sections, oriented N70 and spaced ~20 to 30 km apart, covering the Yemeni part of the margin (Doornenbal *et al.*, 1991). We used 84 exploration wells (located onshore and offshore mainly in the shelf domain), 61 shallow wells (located onshore), and outcrops for the calibration of geometries, ages, and sedimentary facies.

3.3 Deep geophysical data

The Moho and Conrad discontinuities along crustal-scale cross-sections were constrained on previously published datasets including wide-angle seismic profiles (Gaulier *et al.*, 1988;

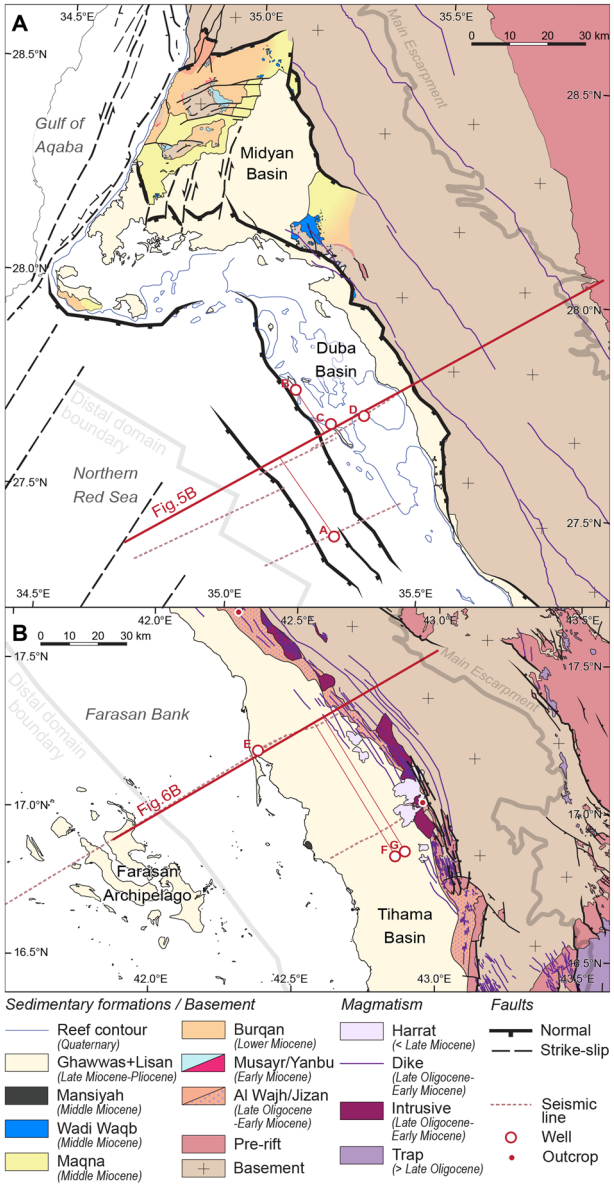

Fig. 3. Geological maps of the Midyan and Duba basins (A), and the Tihama Basin (B). Gulf of Aqaba faults from Ribot *et al.* (2021). See Figure 2C for location. The red lines show trace of the two crustal-scale cross-sections presented in this study. Projection system: Ain el Abd 1970, Aramco, Lambert 2.

Rihm *et al.*, 1991; Voggenreiter *et al.*, 1988), and teleseismic data (Ahmed *et al.*, 2013; Al-Damegh *et al.*, 2005; Hansen *et al.*, 2007). The datasets used to estimate the crustal thickness of the Red Sea (Fig. 1A) are referenced and located in Supp. Data 1.

3.4 Magnetic data

The magnetic anomaly maps used in this study are a compilation of several published datasets, including Cochran (2005) in the northern Red Sea, Zahran *et al.* (2003) for the central Red Sea and the Arabian Shield, and Hall (1979) for the southern Red Sea.

4 Results

4.1 Surface observations

4.1.1 Topography

Onshore morphology is typical of an elevated passive margin with an escarpment delimiting a flat coastal plain from a high plateau gently tilted to the east (Fig. 2A). The escarpment is highly dissected in the north with a mean elevation of ~1000 m, whereas a steep, linear escarpment with a mean elevation of ~2000 m characterizes the south. The transition at the latitude of Jeddah (21.5°N) is abrupt (Fig. 2D). Offshore, a similar segmentation is shown by the bathymetry, with a narrow (25–50 km) continental shelf in the north widening to 100–150 km south of Jeddah, where young oceanic crust (<5 Ma) is exposed in the central trough (Fig. 2A).

4.1.2 Magnetic survey

In the southern Red Sea, the magnetic data shows short-wavelength magnetic anomalies along the central trough, flanked by broader, symmetrical anomalies that extend beyond the distal crustal domain up to the coastal plain (Fig. 2B). These so-called marginal magnetic anomalies below the coastal plain terminate at the latitude of Jeddah, with a sharp transition (×10 km) to the northern highly faulted segment where the anomalies are small, discontinuous, and chaotic (Figs. 2B and 2C).

4.2 Subsurface observations

Major rift faults onshore were mapped by integrating field geology with seismic reflection data (Figs. 2C and 4). It shows that, north of Jeddah (21.5°N), the proximal necking domain along the margin consists of half-grabens tilted towards the continent. To the south, the bounding normal faults disappear and the syn-rift sedimentary strata are tilted seaward in a long-wavelength flexure along the coastal plain (Ghawwas and Tihama basins). This shift in rift polarity coincides with northeast-trending shear zones and sutures in the continental basement (Ad Damm shear zone, Fatima shear zone, and Bi'r Umq suture) mirrored offshore by the Jeddah Fracture Zone (Figs. 2C and 4), and it emphasizes the along-strike segmentation in the topography (Fig. 2D).

4.3 Structural and stratigraphic architecture

We constructed two cross-sections detailing the structural architecture and sedimentary geometries of the northern and southern necking domains of the eastern margin (Figs. 5 and 6). These illustrate the evolution stages of a rifted margin as tectonic sequences defined by seismic units whose distinction is based on their geometry (*e.g.*, growth wedges, sealing faults, reflector terminations). The seismic data generally illuminates the entire sedimentary section, but volcanic sequences and the transition to the distal domain are poorly resolved. The northern section (Fig. 5) is built from four seismic reflection profiles projected orthogonally along the trace (Fig. 3A). It is constrained by four wells (with well logs, cuttings, and biostratigraphic reports) penetrating the entire sedimentary succession from pre-rift to post-rift strata (Fig. 5D). The

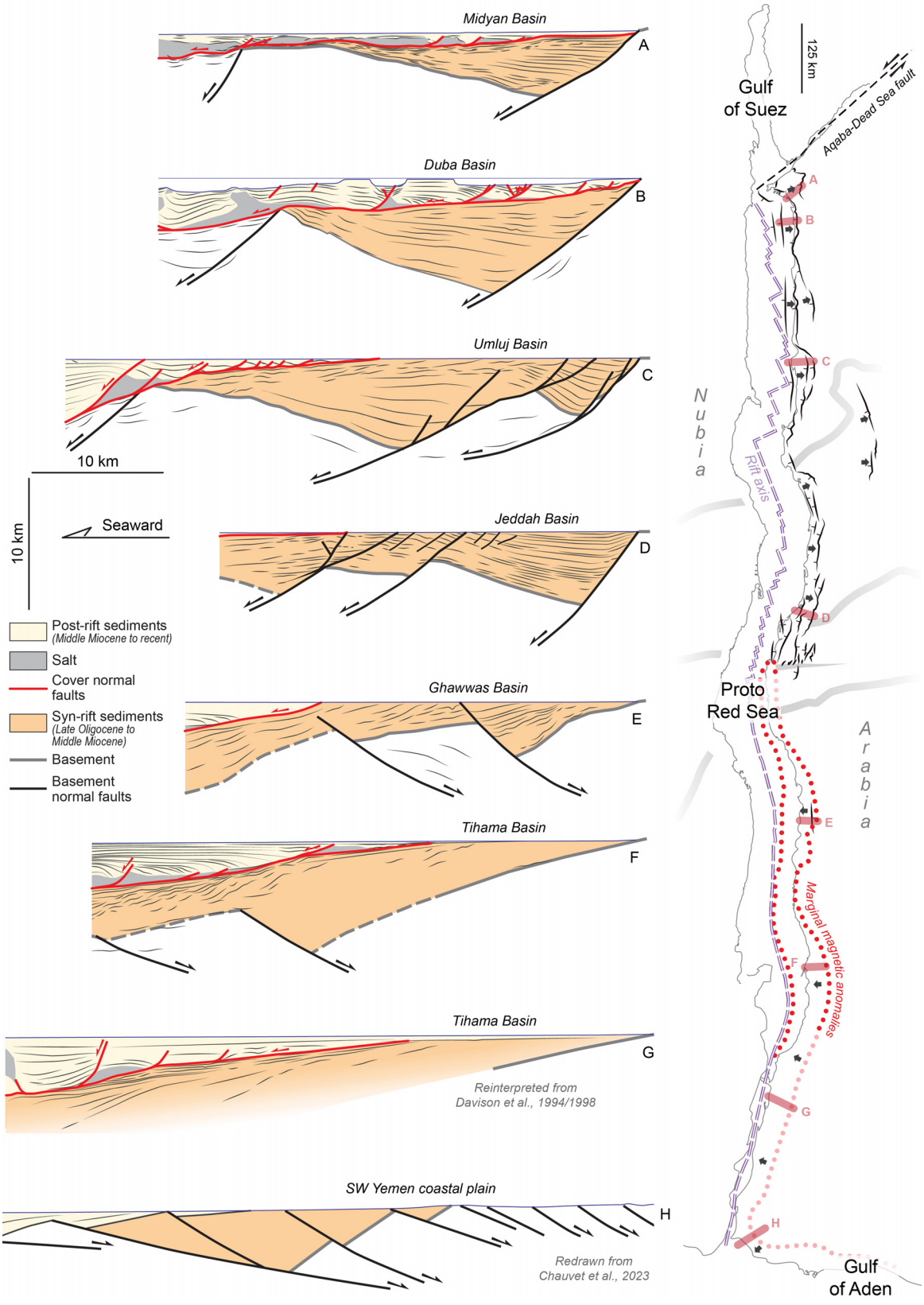

Fig. 4. Interpreted seismic profiles and cross-section illustrating the along-strike structural variability of the necking domain of the margin. To the right, palinspastic restoration of the Red Sea at ~14 Ma showing the main structural elements from Figure 2 and the location of the sections. Black arrows show the dip direction of the syn-rift sediments. Nubia is considered as fix in this reconstruction. Rotation pole from Delaunay *et al.* (2023) (Nubia-Arabia) and Reilinger and McClusky (2011) (Nubia-Danakil).

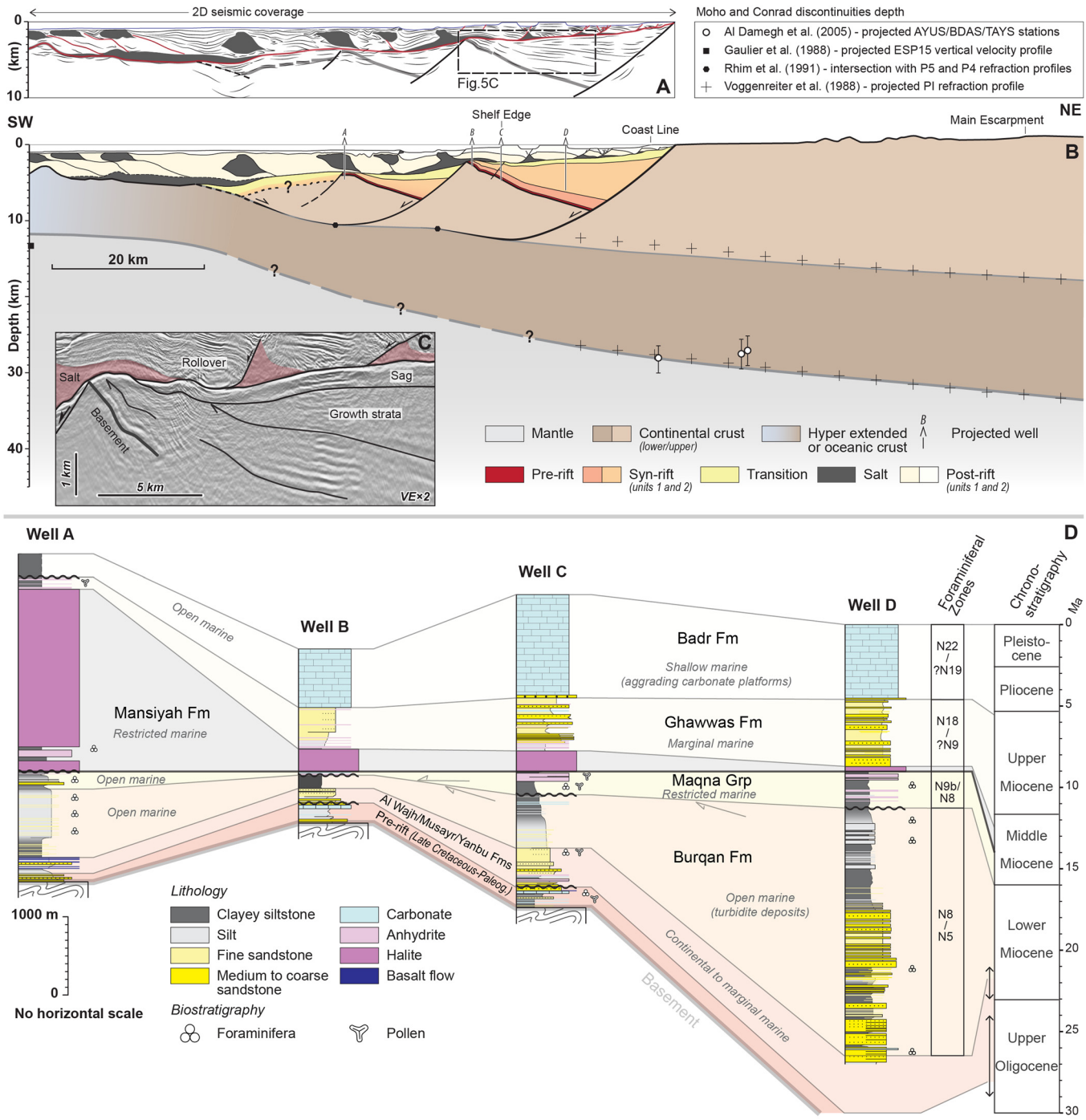

Fig. 5. Structural interpretation of a depth-converted composite seismic reflection profile (line drawing (A)) across the eastern necking domain of the northern Red Sea. The section is calibrated by four exploration wells. The transition between the necking and the distal crustal domains is constrained by the tectonic model of Delaunay *et al.* (2023). The correlation (D) is flattened at the base of the Salt Unit (Mansiyah Fm). See Figure 3A for location.

southern section (Fig. 6) is built from three seismic reflection profiles (Fig. 3B). It is constrained by one well (with well logs, cuttings, and biostratigraphic reports) reaching the upper syn-rift as well as two shallow wells (with cuttings, and biostratigraphic reports) and onshore outcrops of the Tihama Basin (Fig. 6D).

4.3.1 Northern segment

The composite seismic profile (Fig. 5A) shows two tilted blocks bounded by synthetic normal faults affecting pre-rift sediments and the upper crust that are interpreted as rooted in a mid-crustal detachment (Fig. 5B). To the west, syn-rift

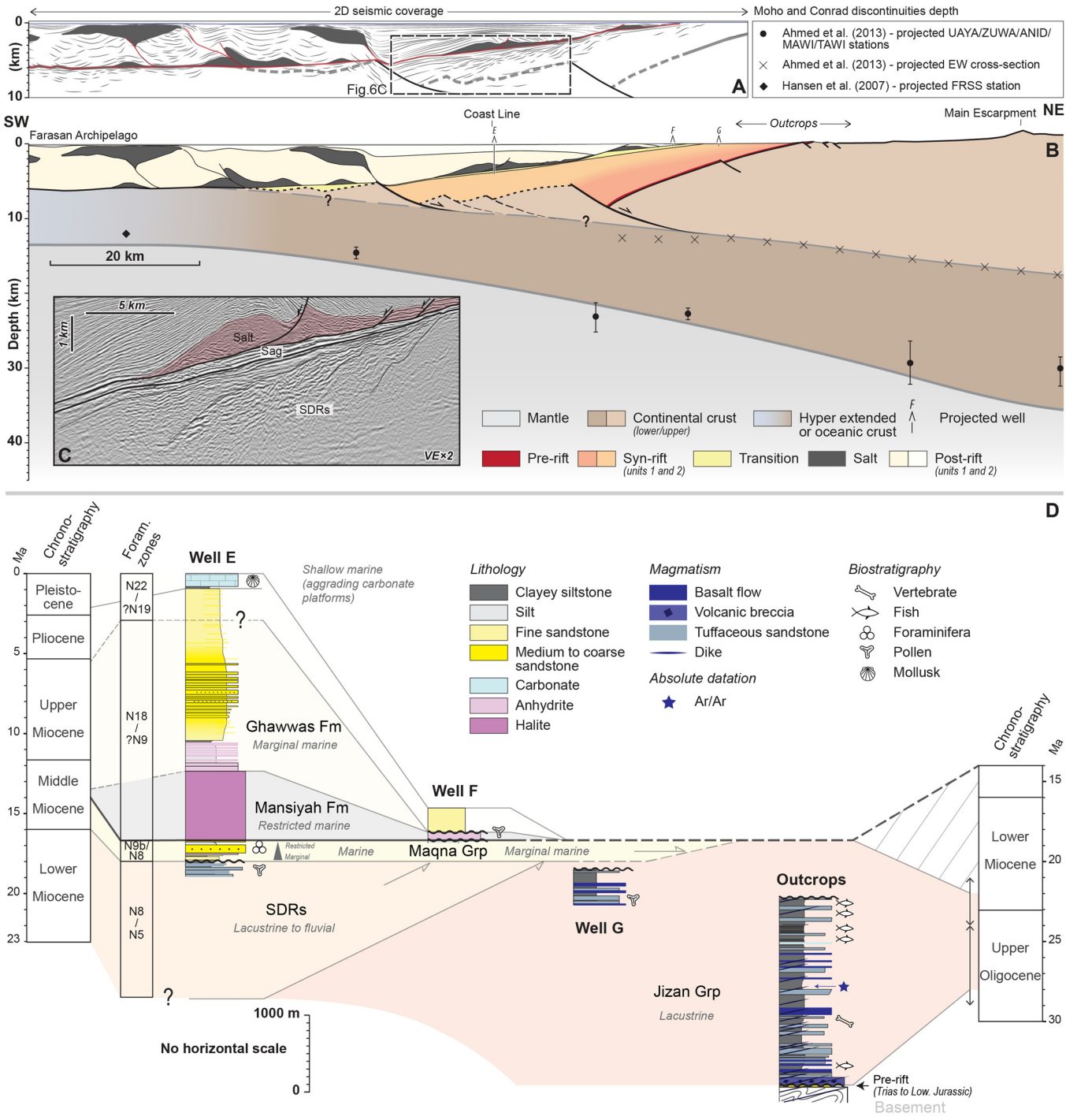

Fig. 6. Structural interpretation of a depth-converted composite seismic reflection profile (line drawing (A)) across the eastern necking domain of the southern Red Sea. The section is calibrated by one exploration well, two shallow wells and outcrop observations. The transition between the necking and the distal crustal domains is constrained by the tectonic model of Delaunay *et al.* (2023). Outcrop synthetic section from Gillman (1968) and Schmidt *et al.* (1983). The correlation (D) is flattened at the base of the Salt Unit (Mansiyah Fm). See Figure 3B for location.

sediments unconformably overly a hyper-thinned crust of unknown nature.

We hereby define two syn-rift units (Fig. 5B). While the occurrence of syn-rift unit 1 in the western half-graben is unclear, in the easternmost half-graben, it consists primarily of ~1400 m thick fluvial to marginal marine deposits along the hanging-wall. This unit, barren of fossils, is correlated to the Late Oligocene-lowermost Miocene Al Wajh and Musayr formations (Fig. 5D) outcropping in the Midyan Basin (Fig. 3A), recording 8 Myr of sedimentation at a mean rate of 0.175 km/Myr. The syn-rift unit 2 consists of ~5000 m thick siliciclastic turbidites deposited along the hanging-wall in a deep marine environment. This Early Miocene unit (N5 to N8 biozones) corresponds to the Burqan Formation (Fig. 5D) with a duration of about 5 Myr and therefore a mean sedimentation rate of 1 km/Myr. The abrupt change from marginal to deep marine environment and the increase of sedimentation rate indicate a significant increase in accommodation rates in the basin. This probably reflects higher tectonic subsidence rates, indicating the climax of the rifting phase.

Above, the sediments show sag-type geometries that unconformably overlie syn-rift sediments in the eastern half-graben (Fig. 5C) while in the western one, wedging persists. We define this unit as a transition unit. Silts with interbedded evaporites dominate the lithology, suggesting a restricted marine environment. Biostratigraphic data indicated a Middle Miocene age (N8 to N9 biozones) that correlates onshore with the Maqna Group (Fig. 5D). The massive salt of the Mansiyah Formation, highly remobilized into diapirs and rollovers, seals the basement faults and unconformably overlies the previously deposited sediments. The good preservation of the upslope extensional domain suggests an initial sag-type geometry with a thickness of >1000 m in the proximal area.

Above sediments are not affected by basement faults and are therefore interpreted as post-rift. The post-rift unit 1 is made of interbedded coarse-grained sandstones and anhydrites (layered evaporites) deposited in a restricted, shallow marine environment. It correlates with the Middle-Late Miocene Ghawwas Formation recently dated between 13.2 Ma and 5 Ma (Pensa *et al.*, 2023). Unconformably above, the post-rift unit 2 consists of Plio-Quaternary massive carbonate platforms growing above the eastern half-graben, defined as the Badr Formation, laterally passing to siliciclastic and pelagic sediments (Fig. 5D).

4.3.2 Southern segment

Contrary to the north, the southern segment is characterized by seaward tilted wedges accommodated by antithetic normal faults rooted in a mid-crustal detachment (Figs. 4 and 6). The proximal wedges show low arcuate reflectors characteristic of inner SDRs. The eroded top of this inner SDR system outcrops along the Tihama Basin as the Jizan Group (Fig. 3B), which is composed of lacustrine deposits interbedded with volcanoclastic sediments and basalt flows (Fig. 6D). Mammal and fish fossils (Madden *et al.*, 1983) combined with radiometric ages on dikes intruding the series (Sebai *et al.*, 1991) suggest an Oligocene age contemporaneous to syn-rift unit 1 (Al Wajh Formation) of the northern segment (Fig. 6D).

Westward, the wedges show more arcuate geometries (Fig. 6C). The Well E shows similar lithologies and environments as the inner SDRs (Fig. 6D). Unconformably above, the first post-SDRs unit shows sag-type geometries (Fig. 6C), made of silty sediments interlayered with evaporites at the base passing upward to slope deposits suggesting a retrogradational trend in a restricted marine environment (Fig. 6D). These sub-horizontal geometries pass to progradational geometries to the east, suggesting more proximal (deltaic) environments. Biostratigraphic data indicate a Middle Miocene age (N8-N9 biozones) equivalent to the transition unit defined for the northern section (Maqna Group). As observed in the northern segment, wedging seems to persist to the west of the section suggesting the emplacement of more distal SDRs contemporaneous with a slowdown of the tectonic/magmatic activity in the proximal necking crustal domain. Similarly to the northern segment, salt-related structures, controlling the post-rift geometries of the basin at the second order, unconformably overly the syn-rift SDRs and the transition unit.

The marginal magnetic anomalies mapped on Figure 2B along the Ghawwas and Tihama coastal basins are likely related to the progressive east-west emplacement and cooling of the SDR wedges during the rift and the transition stages of the necking domain of the margin. Seismic sections and field observations of the Yemen coastal plain also reveal SDRs geometries (Davison *et al.*, 1994; Davison *et al.*, 1998; Chauvet *et al.*, 2023) proving that the southern segment of the eastern Red Sea margin is magma-rich along its entire length (Fig. 4).

5 Discussion

5.1 Segmentation of the eastern Red Sea margin

The eastern necking crustal domain of the Red Sea is divided into two distinct segments, each characterized by specific structural geometries and stratigraphic patterns (Fig. 4). The northern segment (28°N-21.5°N) shows 2-3 tilted blocks separated by synthetic normal faults filled with siliciclastic sediments (Fig. 5). In contrast, the southern segment (21.5°N−13°N) displays seaward tilted sedimentary wedges accommodated by low-angle antithetic faults interpreted as SDRs (Fig. 6A). Field observations and well data show that these wedges are mainly composed of siliciclastic and volcanoclastic sediments with interbedded lava flows (Fig. 6B). Geological observations on the western conjugate margin are consistent with these findings. In the northern Red Sea, seismic reflection and well data confirm the presence of landward-tilted blocks with siliciclastic-dominated syn-tectonic sedimentation (Ali *et al.*, 2023a). Conversely, in the southern Red Sea and Afar region, surface geological observations reveal seaward-tilted syn-rift series composed of siliciclastic/volcanoclastic deposits interbedded with volcanic flows (*e.g.*, Sagri *et al.*, 1998; Stab *et al.*, 2016; Chauvet *et al.*, 2023).

Surface observations indicate that the structural segmentation of the eastern necking crustal domain of the Red Sea is imprinted in the present-day morphology of the continental shelf (Fig. 2A). The stepped configuration of the northern segment is controlled by the location of the 2–3 tilted blocks, with the first defining a narrow continental shelf with aggrading carbonate platforms (Fig. 5). In contrast, the flatter topography inherited from the magma-rich southern segment

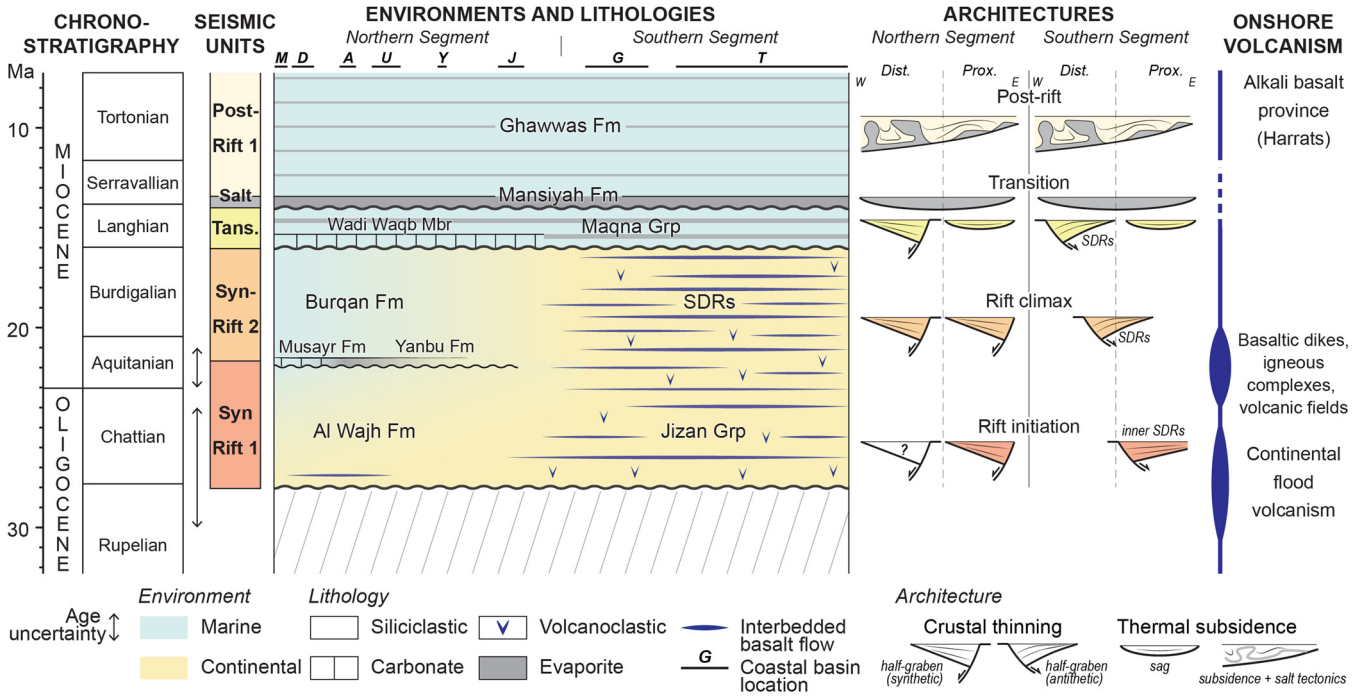

Fig. 7. Synthetic chart with the latitudinal tectonostratigraphic evolution of the necking crustal domain of the eastern margin of the Red Sea showing the main environments, lithologies and basin architectures through time. Seismic units and onshore volcanism are also shown. See Figure 2A for coastal basin location. M: Midyan, D: Duba, A: Azlam, U: Umluj, Y: Yanbu, J: Jeddah, G: Ghawwas, T: Tihama.

results in a much wider continental shelf (Fig. 6). The widening of the western continental shelf towards the south corroborates these observations, suggesting, when combined with geological observations, a first-order symmetric structural pattern of the Red Sea.

The transition between the northern and southern Red Sea segments is sharp and occurs at the latitude of a pre-existing lithospheric structure (Ad Damm shear zone, Fatima shear zone, and Bi'r Umq suture, Fig. 2C) that plays a crucial role in the rift morphology (*e.g.*, Molnar *et al.*, 2020; Stern and Johnson, 2019). The dip reversal in the rift faults is coincident to the latitudinal magmatic budget of the margin. Guan *et al.* (2021) suggested that these deeply rooted basement structures evolving offshore in the Jeddah Fracture Zone could act as a physical barrier, limiting the northward extension of the East-Africa hotspot influence and thus controlling the distribution of magma. Although more gradual in the magmatic intensity along the margins, a similar magmatic gradient has been documented from west to east in the Gulf of Aden (Tard *et al.*, 1991; Nonn *et al.*, 2019).

5.2 Tectonostratigraphic evolution of the eastern Red Sea margin

Four tectonostratigraphic sequences have been recognized over the entire eastern Red Sea necking crustal domain. On both segments, it can be summarized as follows (Fig. 7):

1 28-21 Ma – Rift initiation, in a continental environment, accommodated by seaward dipping normal faults in the northern segment, while inner SDRs were established on the southern segment (Jizan Group).

2 21-16 Ma – Rift climax, marked by an increase of the accommodation rates along the northern segment leading to a progressive marine flooding from the north (Burqan Formation). At the same time, more distal SDRs were formed along the southern segment in continental environments.

3 16-13 Ma – A transition stage, during which the entire margin passes to a marine environment, although confined, as indicated by the presence of evaporites (Maqna Group). Sag-type geometries deposited above a regional unconformity mark a slowing of upper crustal deformation in the proximal part of the necking crustal domain, while syn-rift geometries persist in its distal part. This transitional period ends with the precipitation of massive salt throughout the basin (Mansiyah Formation).

4 13-0 Ma – A post-rift stage where sediments are not affected by basement faults (Ghawwas Formation). The Salt Unit is remobilized and controls the second-order geometry of the post-rift sedimentation.

5.3 Implications for the nature of the distal crustal domain of the Red Sea

Some of our key observations include (1) a progressive cessation of basement fault activity and magmatism in the necking crustal domain of the eastern margin of the Red Sea from 16 to 13 Ma as the Transition and the Salt units deposited followed by (2) a synchronous stratigraphic evolution since then (Fig. 7). The seismic data available in the literature on the conjugate margin (*e.g.*, Izzeldin, 1987; Sang *et al.*, 2023; Ali *et al.*, 2023a,b) shows a similar trend, with an omnipresent

layer of massive salt and post-salt sediments, not affected by basement faults except locally by strike-slip faults in the northern Red Sea, related to the Aqaba-Dead Sea strike-slip system (*e.g.*, Stockli and Bosworth, 2019; Afifi *et al.*, 2023). This suggests that the tectonic subsidence mechanism is comparable on the two conjugate margins of the Red Sea since 16-13 Myr. This implies that from north to south of the Red Sea, (i) the distal crustal domain has formed since the Middle Miocene, and (ii) the nature of the crust of this domain may share similarities.

The magnetic data available in the region suggest conversely a segmentation of this crustal domain between the northern Red Sea, characterized by chaotic and discontinuous magnetic anomalies, and the south, characterized by symmetrical magnetic anomalies on both sides of the axial ridge (Fig. 2B). As the magnetic data provides information on the nature of the crust, it is difficult to reconcile a homogeneous crust throughout with such different magnetic patterns.

This problematic was addressed in previous studies, suggesting that, the low-amplitude anomalies observed away from the ridge axis were due to magma extrusion below a thick sediment cover (*e.g.*, Levi and Riddihough, 1986; Okwokwo *et al.*, 2022), and that the chaotic pattern observed to the north was a combination of intrusions below a sediment cover associated with intense segmentation of the seafloor by transform faults (Delaunay *et al.*, 2023).

In our opinion, other possibilities could also reconcile the pattern of the magnetic anomalies with our observations by considering that the distal crustal domain could be segmented similarly to the necking crustal domains. For example, and following the “main rift" model, we can assume that this crustal domain is hyper-extended continental crust with a true oceanic crust limited to the axis of the Red Sea. In this case, the magnetic anomalies of the southern Red Sea would be due to intensive magma intrusions, in light for example with what was described in the Iberia-Newfoundland magma-poor rifted margin system (Bronner *et al.*, 2011) and on the Namibian magma-rich rifted margin of the South Atlantic (Geoffroy *et al.*, 2022). The northern segment, away from the influence of the East-African hotspot would have been less intruded, not allowing for the onset of linear magnetic anomalies. Alternatively, and following the “main ocean” model, the distal crustal domain of the southern Red Sea could be entirely made-up of oceanic crust, while a proto-oceanic crust could form the distal crustal domain of the northern Red Sea. This type of oceanic crust with anomalous vertical velocities and chaotic magnetic patterns has been previously described in the Gulf of Lyon margin (*e.g.*, Moulin *et al.*, 2015), the Brazilian margin (*e.g.*, Klingelhoefer *et al.*, 2015), and the North American margin (*e.g.*, Bécel *et al.*, 2020). It is interpreted to form during a phase of transient and unfocused melt supply at very slow spreading rates, compatible with the ultra-slow spreading rates of the northern Red Sea (Chu and Gordon, 1998).

The complexity of the nature of the transitional domains of the rifted margins, which is increasingly well documented by recent geophysical data (*e.g.*, Sapin *et al.*, 2021), is enhanced in the Red Sea by the evaporite-rich sedimentary cover and the structural complexity of the Jeddah and Zabargad fracture zones. Therefore, concluding on the nature of the Red Sea distal crustal domain would ultimately lead to oversimplifications. This debate can only be properly addressed with a dense set of combined multi-channel and wide-angle seismic profiles across the northern, central and southern Red Sea.

6 Conclusions

The eastern necking crustal domain of the Red Sea formed between ~28 and ~13 Ma. This domain is segmented between a magma-poor northern segment with tilted blocks filled with siliciclastic sediments, and a magma-rich southern segment with SDRs. Deformation and magmatic activity migrated towards the distal necking crustal domain from ~16 to ~14 Ma. The precipitation of a thick layer of massive salt between ~14 and ~13 Ma marks the onset of the formation of the distal crustal domain along the margin and the cessation of tectonic and magmatic activity in the necking domain. The stratigraphy becomes similar from north to south suggesting similarities in the subsidence mechanisms and therefore in the nature of the crust, discarding the hypothesis that the Red Sea is at different stages of rifting from north to south.

Supplementary material

SUPPLEMENTARY DATA 1: A) Seismic refraction surveys and teleseismic data location. B) Seismic reflection surveys location. C) Moho depth map. D) Top to the acoustic basement depth map. Offshore Eritrea area (speculative) is extrapolated by symmetry from the eastern Red Sea margin. E) Crustal thickness map constructed by subtracting the top to the basement map (D) from the Moho depth map (C).

The Supplementary Material is available at https://www.bsgf.fr/10.1051/bsgf/2024009/olm.

Acknowledgments

This study was completed under KAUST’s Competitive Research Grant 4082 on “Geologic Evolution of the Red Sea and Gulf of Aqaba”. Petroleum companies operating in the Red Sea are acknowledged for the opportunity to interpret their data for scientific purposes. We thank Petroleum Experts (Petex) for providing an academic licence of the Move software for structural modelling.

Finally, we would like to thank two anonymous reviewers for their insightful reviews that greatly improved the quality on the manuscript.

References

Afifi AS, Moustafa AR, Helmy HM. 2023. Rift domains and structural framework of the northwestern Red Sea basin, Egypt. *Int J Earth Sci* 112: 2049–2064.

Augustin N, Van Der Zwan FM, Devey CW, Brandsdóttir B. 2021. 13 million years of seafloor spreading throughout the Red Sea Basin. *Nat Commun* 12: 2427.

Ahmed A, Tiberi C, Leroy S, Stuart GW, Keir D, Sholan J, Khanbari K, Al-Ganad I, Basuyau C. 2013. Crustal structure of the rifted volcanic margins and uplifted plateau of Western Yemen from receiver function analysis. *Geophys J Int* 193: 1673–1690.

Al-Damegh K, Sandvol E, Barazangi M. 2005. Crustal structure of the Arabian plate: new constraints from the analysis of teleseismic receiver functions. *Earth Planet Sci Lett* 231: 177–196.

Ali M, Decarlis A, Ligi M, Ball P, Bosworth B, Ceriani A. 2023. Red Sea rifting in central Egypt: constraints from the offshore Quseir province.
J Geol Soc 180: jgs2022–2105.

Ali M, Koyi H, Bosworth W, Ligi M, Ball PJ, Decarlis A. 2023. Geometry and kinematics of the Middle to Late Miocene salt tectonics, central Egyptian Red Sea margin. *J Struct Geol* 176: 104955.

Aslanian D, Moulin M, Olivet J-L., Unternehr P, Matias L, Bache F, Rabineau M, Nouzé H, Klingelheofer F, Contrucci I. 2009. Brazilian and African passive margins of the Central Segment of the South Atlantic Ocean: kinematic constraints. *Tectonophysics* 468: 98–112.

Bally AW, Snelson S, 1980. Realms of subsidence, in Miall AD, ed., *Facts and Principles of World Petroleum Occurrence*, *Mem. −Can. Soc. Pet. Geol*. 6, 9–94.

Bellahsen N, Faccenna C, Funiciello F, Daniel JM, Jolivet L. 2003. Why did Arabia separate from Africa? Insights from 3-D laboratory experiments. *Earth Planet Sci Lett* 216: 365–381.

Beydoun ZR. 1989. The hydrocarbon prospects of the Red Sea-Gulf of Aden: a review. *J Petrol Geol* 12: 125–144.

Bécel, A., Davis, J. K., Shuck, B. D., Van Avendonk, H. J. A., & Gibson, J. C. (2020). Evidence for a prolonged continental breakup resulting from slow extension rates at the eastern north American volcanic rifted margin. Journal of Geophysical Research: Solid Earth, 125, e2020JB020093. https://doi.org/10.1029/2020JB020093

Bohannon RG. 1987. Tectonic configuration of the Western Arabian Continental Margin, Southern Red Sea, Kingdom of Saudi Arabia, *Open-File Report*, p. 28.

Bohannon RG, Naeser CW, Schmidt DL, Zimmermann RA. 1989. The timing of uplift, volcanism, and rifting peripheral to the Red Sea: a case for passive rifting? *J Geophys Res* 94: 1683–1701.

Bosworth W. 1995. A high-strain rift model for the southern Gulf of Suez (Egypt). *Geological Society, London, Special Publications* 80, 75–102.

Bosworth W. 2015. Geological Evolution of the Red Sea: Historical Background, Review, and Synthesis. In: Rasul, N.M.A., Stewart, I. C.F., Eds. The Red Sea: The Formation, Morphology, Oceanography and Environment of a Young Ocean Basin. Springer Berlin Heidelberg, Berlin, Heidelberg, pp. 45-78.

Bosworth W, Huchon P, McClay K. 2005. The Red Sea and Gulf of Aden basins. *J Afr Earth Sci* 43: 334–378.

Bosworth W, Stockli DF. 2016. Early magmatism in the greater Red Sea rift: timing and significance. *Can J Earth Sci* 53: 1158–1176.

Bronner A, Sauter D, Manatschal G, Péron-Pinvidic G, and Munschy M. 2011. Magmatic breakup as an explanation for magnetic anomalies at magma-poor rifted margins. *Nat Geosci* 4: 549–553.

Bunter MAG, Abdel Magid AEM. 1989. The Sudanese red sea: 1. New developments in stratigraphy and petroleum-geological evolution. *J Petrol Geol* 12: 145–166.

Camp VE, Roobol MJ. 1992. Upwelling Asthenosphere beneath Western Arabia and its regional implications. *J Geophys Res Solid Earth* 97: 15255–15271.

Chauvet F, Geoffroy L, Le Gall B, Jaud M. 2023. Volcanic passive margins and break-up processes in the southern Red Sea. *Gondwana Res* 117: 169–193.

Chenin P, Manatschal G, Ghienne JF, Chao P. 2022. The syn-rift tectono-stratigraphic record of rifted margins (Part II): a new model to break through the proximal/distal interpretation frontier. *Basin Res* 34: 489–532.

Chu, D., & Gordon, R. G. (1998). Current plate motions across the Red Sea. Geophysical Journal International, 135, 2, 313–328. https://doi.org/10.1046/j.1365-246X.1998.00658.x

Cochran JR. 2005. Northern Red Sea: Nucleation of an oceanic spreading center within a continental rift. *Geochem Geophys Geosyst* 6.

Courtillot V, Armijo R, Tapponnier P. 1987. The Sinai Triple Junction Revisited. *Tectonophysics* 141, 181–190.

Davison I, Alkadasi M, Alkhirbash S, Alsubbary AK, Baker J, Blakey S, Bosence D, Dart C, Heaton R, McClay K, Menzies M, Nichols G, Owen L, Yelland A. 1994. Geological evolution of the southeastern Red-Sea Rift Margin, Republic of Yemen. *Geol Soc Am Bull* 106: 1474–1493.

Davison I, Bosence D, Alsop GI, Al-Aawah MH. 1996. Deformation and sedimentation around active Miocene salt diapirs on the Tihama Plain, northwest Yemen. *Geolog Soc Lond Spec Publ* 100: 23–39.

Davison I, Tatnell MR, Owen LA, Jenkins G, Baker J. 1998. Tectonic geomorphology and rates of crustal processes along the Red Sea margin, north-west Yemen. In: Purser BH, Bosence, D.W.J., Eds. Sedimentation and Tectonics in Rift Basins: Red Sea − Gulf of Aden. Dordrecht: Springer, pp. 595–612.

Delaunay A, Baby G, Fedorik J, Afifi AM, Tapponnier P, Dyment J. 2023. Structure and morphology of the Red Sea, from the mid-ocean ridge to the ocean-continent boundary. *Tectonophysics* 849: 229728.

Doornenbal JC, DeGroot, P.F.L., Saif SM, Schroot BM, 1991. Geology and Hydrocarbon Potential of the Tihama Basin, Republic of Yemen, Middle East Oil Show. OnePetro, Bahrain.

Dullo W-C., Hötzl H, Jado AR. 1983. New stratigraphical results from the Tertiary sequence of the Midyan area, NW Saudi Arabia. *Newslett Stratigr* 12: 75–83.

Egloff F, Rihm R, Makris J, Izzeldin Y, Bobsien M, Meier K, Junge P, Noman T, Warsi W. 1991. Contrasting structural styles of the eastern and western margins of the southern Red Sea: the 1988 SONNE experiment. *Tectonophysics* 198: 329–353.

Evans AL. 1988. Neogene tectonic and stratigraphic events in the Gulf of Suez rift area, Egypt. *Tectonophysics* 153: 235–247.

Gaulier JM, Lepichon X, Lyberis N, Avedik F, Geli L, Moretti I, Deschamps A, Hafez S. 1988. Seismic study of the crust of the northern Red Sea and Gulf of Suez. *Tectonophysics* 153: 55–88.

Gawthorpe RL, Leeder MR. 2000. Tectono-sedimentary evolution of active extensional basins. *Basin Res* 12: 195–218.

Geoffroy L, Chauvet F, Ringenbach J-C. 2022. Middle-lower continental crust exhumed at the distal edges of volcanic passive margins. *Commun Earth Environ* 3: 95.

Gillman M. 1968. Primary results of a geological and geophysical reconnaissance of the Jizan coastal plain in Saudi Arabia, Regional Technical Symposium. OnePetro, Dahran, Saudi Arabia.

Guan HX, Geoffroy L, Xu M. 2021. Magma-assisted fragmentation of Pangea: continental breakup initiation and propagation. *Gondwana Res* 96: 56–75.

Guennoc P, Pouit G, Nawab Z. 1988. Chapter 39 − The Red Sea: history and associated mineralization. In: Manspeizer W, Ed. Developments in Geotectonics. Elsevier, pp. 957–982.

Hall SA. 1979. A total intensity magnetic anomaly map of the Red Sea and its interpretation, Open-File Report.

Hansen SE, Rodgers AJ, Schwartz SY, Al-Amri AMS. 2007. Imaging ruptured lithosphere beneath the Red Sea and Arabian Peninsula. *Earth Planet Sci Lett* 259: 256–265.

Haupert I, Manatschal G, Decarlis A, Unternehr P. 2016. Upper-plate magma-poor rifted margins: Stratigraphic architecture and structural evolution. *Mar Petrol Geol* 69: 241–261.

Heaton RC, Jackson MPA, Bamahmoud M, Nani ASO. 1995. Superposed Neogene extension, contraction, and salt canopy emplacement in the Yemeni Red Sea. In: Jackson MPA, Roberts DG,Snelson S, Eds. Salt tectonics: a global perspective: AAPG Memoir 65. The American Association of Petroleum Geologists, pp. 333–351.

Hughes GW, Johnson RS. 2005. Lithostratigraphy of the Red Sea region. *Geoarabia* 10: 49–126.

Issachar R, Gómez-García ÁM, Ebbing J. 2023. Lithospheric structure of the Red Sea based on 3D density modeling: a contrasting rift architecture. *J Geophys Res: Solid Earth* 128: e2022J B025458.

Izzeldin AY. 1987. Seismic, gravity and magnetic surveys in the central part of the Red Sea: their interpretation and implications for the structure and evolution of the Red Sea. *Tectonophysics* 143: 269–306.

Klingelhoefer F, Evain M, Afilhado A, Rigoti C, Loureiro A, Alves D, Leprêtre A, Moulin M, Schnurle P, Benabdellouahed M, Baltzer A, Rabineau M, Feld A, Viana A, Aslanian D. 2014. Imaging proto-oceanic crust off the Brazilian Continental Margin. *Geophys J Int* 200: 471–488.

Korostelev F, Weemstra C, Leroy S, Boschi L, Keir D, Ren Y, Molinari I, Ahmed A, Stuart GW, Rolandone F, Khanbari K, Hammond JOS, Kendall JM, Doubre C, Ganad IA, Goitom B, Ayele A. 2015. Magmatism on rift flanks: insights from ambient noise phase velocity in Afar region. *Geophys Res Lett* 42: 2179–2188.

Kruck W, Schäffer U, Thiele J. 1996. Explanatory notes on the geological map of the Republic of Yemen: western part (former Yemen Arab Republic). Schweizerbart Science Publishers, Stuttgard, Germany.

Le Magoarou C, Hirsch K, Fleury C, Martin R, Ramirez-Bernal J, Ball P. 2021. Integration of gravity, magnetic, and seismic data for subsalt modeling in the Northern Red Sea. *Interpretation* 9: T507–T521.

Le Pichon X, Gaulier JM. 1988. The rotation of Arabia and the Levant fault system. *Tectonophysics* 153: 271–294.

Levi S, Riddihough R. 1986. Why are marine magnetic anomalies suppressed over sedimented spreading centers? *Geology* 14: 651–654.

Madden GT, Schmidt DL, Whitmore, Jr., FC. 1983. Mastritherium (Artiodactyla, Anthracotheriidae) from Wadi Sabya, southwestern Saudi Arabia: an earliest Miocene age for continental rift-valley volcanic deposits of the Red Sea margin, Open-File Report, p. 24.

Masini E, Manatschal G, Mohn G. 2013. The Alpine Tethys rifted margins: Reconciling old and new ideas to understand the stratigraphic architecture of magma-poor rifted margins. *Sedimentology* 60: 174–196.

McClusky S, Reilinger R, Ogubazghi G, Amleson A, Healeb B, Vernant P, Sholan J, Fisseha S, Asfaw L, Bendick R, Kogan L. 2010. Kinematics of the southern Red Sea-Afar Triple Junction and implications for plate dynamics. *Geophys Res Lett* 37.

McKenzie DP, Davies D, Molnar P. 1970. Plate tectonics of the Red Sea and East Africa. *Nature* 226: 243–248.

Mitchell DJW, Allen RB, Salama W, Abouzakm A. 1992. Tectonostratigraphic framework and hydrocarbon potential of the red sea. J Petrol Geol 15: 187–210.

Mitchell NC, Shi W, Izzeldin AY, Stewart ICF. 2021. Reconstructing the level of the central Red Sea evaporites at the end of the Miocene. *Basin Res* 33: 1266–1292.

Mohriak W. 2019. Rifting and salt deposition on continental margins: differences and similarities between the red sea and the south atlantic sedimentary basins. In: Rasul NMA, Stewart ICF, Eds. Geological Setting, Palaeoenvironment and Archaeology of the Red Sea. Cham: Springer International Publishing, pp. 159–201.

Molnar N, Cruden A, Betts P. 2020. The role of inherited crustal and lithospheric architecture during the evolution of the Red Sea: insights from three dimensional analogue experiments. *Earth Planet Sci Lett* 544: 116377.

Montenat C, Ott D'Estevou P, Purser B, Burollet, P.-F., Jarrige, J.-J., s., Orszag-Sperber F, Philobbos E, Plaziat J-C., Prat P, Richert J-P., Roussel N, Thiriet J-P. 1988. Tectonic and sedimentary evolution of the Gulf of Suez and the northwestern Red Sea. *Tectonophysics* 153: 161–177.

Moretti I, Colletta B. 1987. Spatial and temporal evolution of the Suez Rift subsidence. *J Geodyn* 151–168.

Moulin M, Klingelhoefer F, Afilhado A, Aslanian D, Schnurle P, Nouzé, H., Rabineau M, Beslier M-O., Feld A. 2015. Deep crustal structure across a young passive margin from wide-angle and reflection seismic data (The SARDINIA Experiment) – I. Gulf of Lion's margin. *Bulletin de la Société Géologique de France* 186 : 309–330.

Neuharth D, Brune S, Wrona T, Glerum A, Braun J, Yuan X. 2022. Evolution of rift systems and their fault networks in response to surface processes. *Tectonics* 41: e2021TC007166.

Nonn C, Leroy S, Lescanne M, Castilla R. 2019. Central Gulf of Aden conjugate margins (Yemen-Somalia): tectono-sedimentary and magmatism evolution in hybrid-type margins. *Mar Petrol Geol*. 105: 100–123.

Nutz A, Ragon T, Schuster M. 2022. Cenozoic tectono-sedimentary evolution of the northern Turkana Depression (East African Rift System) and its significance for continental rifts. *Earth Planet Sci Lett* 578: 117285.

Okwokwo OI, Mitchell NC, Shi W, Stewart, I.C.F., Izzeldin AY. 2022. How have thick evaporites affected early seafloor spreading magnetic anomalies in the Central Red Sea? *Geophys J Int* 229: 1550–1566.

Pensa T, Huertas AD, Aljahdali AH, Afifi AM. 2023. Geological evolution of the post-rift section in the Red Sea basin, The International Meeting for Applied Geoscience & Energy (IMAGE) Houston, USA.

Pérez-Gussinyé M., Andrés-Martínez M, Araújo M, Xin Y, Armitage J, Morgan JP. 2020. Lithospheric strength and rift migration controls on synrift stratigraphy and breakup unconformities at rifted margins: examples from numerical models, the Atlantic and South China Sea Margins. *Tectonics* 39: e2020TC006255.

Phillips JD, Ross DA. 1970. A discussion on the structure and evolution of the Red Sea and the nature of the Red Sea, Gulf of Aden and Ethiopia rift junction – Continuous seismic reflexion profiles in the Red Sea. *Philos Royal Soc London A* 267: 143–152.

Prosser S. 1993. Rift-related linked depositional systems and their seismic expression. Geological Society, *London, Special Publications* 71, 35–66.

Purser BH, Hötzl H. 1988. The sedimentary evolution of the Red Sea rift: a comparison of the northwest (Egyptian) and northeast (Saudi Arabian) margins. *Tectonophysics* 153: 193–208.

Reilinger R, McClusky S. 2011. Nubia-Arabia-Eurasia plate motions and the dynamics of Mediterranean and Middle East tectonics. *Geophys J Int* 186: 971–979.

Ribot M, Klinger Y, Jonsson S, Avsar U, Pons-Branchu E, Matrau R, Mallon FL. 2021. Active faults' geometry in the Gulf of Aqaba,

Southern Dead Sea Fault, Illuminated by Multibeam Bathymetric Data. *Tectonics* 40: e2020TC006443.

Rihm R, Makris J, Möller L. 1991. Seismic surveys in the Northern Red Sea: asymmetric crustal structure. *Tectonophysics* 198: 279–295.

Rime V, Foubert A, Ruch J, Kidane T. 2023. Tectonostratigraphic evolution and significance of the Afar Depression. *Earth-Sci Rev* 244: 104519.

Rohais S, Barrois A, Colletta B, Moretti I. 2016. Pre-salt to salt stratigraphic architecture in a rift basin: insights from a basin-scale study of the Gulf of Suez (Egypt). *Arab J Geosci* 9: 317.

Rowan MG. 2014. Passive-margin salt basins: hyperextension, evaporite deposition, and salt tectonics. *Basin Res* 26: 154–182.

Sagri M, Abbate E, Azzaroli A, Balestrieri ML, Benvenuti M, Bruni P, Fazzuoli M, Ficcarelli G, Marcucci M, Napoleone G. 1998. New data on the Jurassic and Neogene sedimentation in the Danakil Horst and Northern Afar Depression, in: Crasquin-Soleau S, Barrier, E. (Eds.), Memoir 3: stratigraphy and evolution of Peri-Tethyan platforms. Mémoires du Muséum National d'Histoire Naturelle de Paris, pp. 193–214.

Sang Y-D., Adam BMT, Li C-F., Huang L, Wen Y-L., Zhang J-L., Liu Y-T. 2023. Punctiform Breakup and Initial Oceanization in the Central Red Sea Rift. *J Mar Sci Eng* 11: 808.

Sapin F, Ringenbach JC, Clerc C. 2021. Rifted margins classification and forcing parameters. *Sci Rep* 11: 8199.

Savoyat E, Shiferaw A, Balcha T. 1989. Petroleum exploration in the Ethiopian Red Sea. *J Petrol Geol* 12: 187–204.

Schmidt DL, Hadley DG, Brown GF. 1983. Middle Tertiary continental rift and evolution of the Red Sea in southwestern Saudi Arabia, Open-File Report, Reston, VA, p. 56.

Sebai A, Zumbo V, Feraud G, Bertrand H, Hussain AG, Giannerini G, Campredon R 1991. 40Ar/39Ar dating of alkaline and tholeiitic magmatism of Saudi-Arabia related to the early Red-Sea Rifting. *Earth Planet Sci Lett* 104, 473–487.

Stab M, Bellahsen N, Pik R, Quidelleur X, Ayalew D, and Leroy S. 2016. Modes of rifting in magma-rich settings: Tectono-magmatic evolution of Central Afar. *Tectonics* 35, 2–38.

Steckler MS, Watts AB, 1978. Subsidence of the Atlantic-type continental margin off New York. *Earth Planet Sci Letters* 41: 1–13.

Stein CA, Stein S. 1992. A model for the global variation in oceanic depth and heat flow with lithospheric age. *Nature* 359L: 123–129.

Stern RJ, Johnson PR. 2019. Constraining the Opening of the Red Sea: Evidence from the Neoproterozoic Margins and Cenozoic Magmatism for a Volcanic Rifted Margin. In: Rasul, N.M.A., Stewart, I.C.F., Eds. Geological Setting, Palaeoenvironment and Archaeology of the Red Sea. Cham: Springer International Publishing, pp. 53–79.

Stockli DF, Bosworth W. 2019. Timing of Extensional Faulting Along the Magma-Poor Central and Northern Red Sea Rift Margin – Transition from Regional Extension to Necking Along a Hyper-extended Rifted Margin. In: Rasul NMA, Stewart ICF, Eds. Geological Setting, Palaeoenvironment and Archaeology of the Red Sea. Cham: Springer International Publishing, pp. 81–111.

Szymanski E, Stockli DF, Johnson PR, Hager C. 2016. Thermo-chronometric evidence for diffuse extension and two-phase rifting within the Central Arabian Margin of the Red Sea Rift. *Tectonics* 35: 2863–2895.

Tard M, Masse P, Walgenwitz F, Gruneisen P. 1991. The volcanic passive margin in the vicinity of Aden, Yemen. *Bulletin des centres de recherches exploration – Production Elf-Aquitaine* 15: 1–9.

Tubbs REJ, Fouda HGA, Afifi AM, Raterman NS, Hughes GW, Fadolalkarem YK. 2014. Midyan Peninsula, northern Red Sea, Saudi Arabia: seismic imaging and regional interpretation. *Geoarabia* 19: 165–184.

Vicente de Gouveia S, Besse J, Frizon de Lamotte D,Greff-Lefftz M, Lescanne M, Gueydan F, Leparmentier F. 2018. Evidence of hotspot paths below Arabia and the Horn of Africa and consequences on the Red Sea opening. *Earth Planet Sci Lett* 487: 210–220.

Voggenreiter W, Hötzl H, Mechie J, 1988. Low-angle detachment origin for the Red Sea Rift System? *Tectonophysics* 150: 51–75.

Zahran HM, Stewart ICF, Johnson PR, Basahel MH. 2003. Aeromagnetic-anomaly maps of central and western Saudi Arabia, Open-File Report, Saudi Arabia, p. 6.

Cite this article as: Baby G, Delaunay A, Aslanian D, Afifi AM. 2024. The tectonostratigraphic latitudinal record of the eastern Red Sea margin, *BSGF - Earth Sciences Bulletin* 195: 12.